

RESEARCH ARTICLE

10.1002/2015JF003778

Key Points:

- Fluvial channel sedimentation and avulsion location backstep during sea-level rise
- Time to avulsion scales with increasing rate of sea-level rise
- Floodplain capture of sediment is necessary to model influence of base-level rise on stratigraphy

Correspondence to:

K. E. Moran,
kemoran4@gmail.com

Citation:

Moran, K. E., J. A. Nittrouer, M. M. Perillo, J. Lorenzo-Trueba, and J. B. Anderson (2016), Morphodynamic modeling of fluvial channel fill and avulsion time scales during early Holocene transgression, as substantiated by the incised valley stratigraphy of the Trinity River, Texas, *J. Geophys. Res. Earth Surf.*, 121, doi:10.1002/2015JF003778.

Received 1 NOV 2015

Accepted 2 DEC 2016

Accepted article online 7 DEC 2016

Morphodynamic modeling of fluvial channel fill and avulsion time scales during early Holocene transgression, as substantiated by the incised valley stratigraphy of the Trinity River, Texas

Kaitlin E. Moran¹ , Jeffrey A. Nittrouer¹ , Mauricio M. Perillo² , Jorge Lorenzo-Trueba³ , and John B. Anderson¹ 

¹Department of Earth Science, Rice University, Houston, Texas, USA, ²ExxonMobil Upstream Research Company, Spring, Texas, USA, ³Earth and Environmental Studies Department, Montclair State University, Montclair, New Jersey, USA

Abstract The Trinity River system provides a natural laboratory for linking fluvial morphodynamics to stratigraphy produced by sea-level rise, because the sediments occupying the Trinity incised valley are well constrained in terms of timing of deposition and facies distribution. Herein, the Trinity River is modeled for a range of base-level rise rates, avulsion thresholds, and water discharges to explore the effects of backwater-induced in-channel sedimentation on channel avulsion. The findings are compared to observed sediment facies to evaluate the capability of a morphodynamic model to reproduce sediment deposition patterns. Base-level rise produces mobile locations of in-channel sedimentation and deltaic channel avulsions. For scenarios characteristic of early Holocene sea-level rise (4.3 mm yr^{-1}), the Trinity fluvial-deltaic system progrades 13 m yr^{-1} , followed by backstepping of 27 m yr^{-1} . Avulsion is reached at the position of maximum sediment deposition (located 108 km upstream of the outlet) after 3,548 model years, based on sedimentation filling 30% of the channel. Under scenarios of greater base-level rise, avulsion is impeded because the channel fill threshold is never achieved. Accounting for partitioning of bed-material sediment between the channel and floodplain influences the timing and location of avulsion over millennial time scales: the time to avulsion is greatly increased. Sedimentation patterns within the valley, modeled and measured, indicate preference toward sandy bed material, and the rates of deposition are substantiated by previous measurements. Although the results here are specific to the Trinity River, the analysis provides a framework that is adaptable to other lowland fluvial-deltaic systems.

1. Introduction

Morphodynamic models of fluvial systems have been used to evaluate processes influencing channel evolution, by coupling sediment transport and fluid-flow properties. Recently, such models applied to lowland rivers nearing a receiving basin have modified the assumption of uniform flow in order to explore how nonuniform, backwater conditions affect the timing and magnitude of sediment transport, channel filling, and avulsion frequency and location [Parker, 2004; Hoyal and Sheets, 2009; Chatanantavet et al., 2012; Lamb et al., 2012; Nittrouer et al., 2012; Ganti et al., 2014].

For example, Jerolmack and Swenson [2007] proposed that the initiation of backwater regime establishes delta sedimentation and sets the location of distributary channel forming avulsions. Nittrouer et al. [2012] modeled channel sediment deposition within the backwater region of the lowermost Mississippi River, noting that the preferential region of sediment deposition coincides with the location of five major Holocene avulsions and higher rates of channel lateral migration. Lamb et al. [2012] explored the effects of hydraulic drawdown associated with flood-water discharge events connected to an expanding river-mouth plume, showing how this effect could produce channel bed sediment erosion within the lowermost reaches of the Mississippi River. Chatanantavet et al. [2012] expanded on this study by implementing variable water discharge conditions within the modeling framework, which modifies the location of maximum backwater-induced sedimentation rates for the Mississippi River. Chatanantavet et al. [2012] also adapted their model to address the timing of measured Holocene avulsions for the Mississippi system. Most of these previous studies presume a condition of stable base-level and no floodplain-channel sediment exchange, which may be appropriate over the late Holocene and time scales of a few centuries [Lamb et al., 2012; Nittrouer et al., 2012; Ganti et al., 2014]. However, during the early and middle Holocene, fluvial-deltaic systems would have been

influenced by rapidly changing base-level conditions that likely exerted an important influence on backwater-induced sedimentation.

Herein, a numerical model is developed to evaluate a fluvial-deltaic system undergoing transgression due to base-level rise. The central hypothesis is that because morphodynamics of a fluvial system nearing the receiving basin are sensitive to base-level, there will be important spatiotemporal adjustments to sediment transport rates, which in turn modify sediment depositional patterns. In essence, base-level rise will produce accommodation space that is filled by backwater-induced sedimentation. Additionally, because the time scale of early and middle Holocene transgression is long (several thousand years), it is necessary to account for sediment partitioning between the channel and adjacent floodplain, because such exchange processes occur over comparable time scales [Lauer and Parker, 2008a, 2008b, 2008c].

Sea-level rise under conditions of sufficiently low sediment supply increases accommodation space and lends to development of backstepping fluvial-deltaic stratigraphy. The preservation of these deposits is hampered due to transgressive ravinement, which erodes and significantly modifies coastal deposits. However, underfilled incised valleys that are characterized by bays—for example, those found for the modern northern Gulf of Mexico (e.g., Galveston, Sabine, and Mobile)—have a higher preservation potential because the deposits filling the topographic low of a valley are relatively confined and protected from transgressive ravinement [Thomas and Anderson, 1988]. The stratigraphy of incised valleys is therefore useful for assessing fluvial-deltaic sedimentation processes during periods of transgression. For example, previous research from Galveston Bay, Texas, USA (Figure 1), collected seismic data and sediment cores to evaluate the Holocene record for the filling of the Trinity incised valley system, where the timing and spatial patterns of sedimentary facies are well constrained [Anderson et al., 1992, 2008; Thomas and Anderson, 1994; Rodriguez et al., 2005; Simms et al., 2006].

Our study leverages this extensive research on the stratigraphy of the Trinity River system, in order to inform and validate a morphodynamic model that replicates the operation of fluvial-deltaic sedimentation during transgression (sections 2.1 and 2.2). The most basic information required to properly constrain a model is available, including age, distribution, and facies of accumulated sediment, the morphology of the valley, and local sea-level conditions during the Holocene (Figures 1–4) [Anderson et al., 2008; Milliken et al., 2008]. These data afford the opportunity to link morphodynamic processes operating under the influence of transgression to sediment deposition patterns and the production of stratigraphy, by comparing predicted patterns of deposition to the measured sedimentary facies. Although applied to the Trinity River, the model developed here provides a general framework for predicting facies patterns for other fluvial-deltaic systems.

The equations used herein to model morphodynamic interactions of base-level rise and channel-floodplain exchanges have been developed over decades of previous research [De Vries, 1965; Parker et al., 1998a, 1998b, Parker, 2004; Parker et al., 2008a, 2008b]. The contribution of this study lies in the application of such equations to evaluate the combined effects of base-level rise and channel-floodplain sediment partitioning on the spatiotemporal development of fluvial-deltaic sedimentation, and the tendency of these processes to produce channel avulsions. Since the modeling framework is paired with the extensive data of the incised valley stratigraphy of the Trinity River, the location is ideal to test the model outcomes.

2. Background

2.1. Trinity River and Galveston Bay

High-resolution seismic data produced by sparker and boomer systems have been used to construct a detailed map of the sedimentary facies associated with the Trinity incised valley [Anderson et al., 1992; Thomas and Anderson, 1994]. Combined with drill cores, the patterns of the valley infill for this system have been addressed by numerous researchers [e.g., Rodriguez et al., 2005; Simms et al., 2006; Anderson et al., 2008].

The Trinity River (Figure 1) incised valley was down cut during the previous falling stage in sea level during marine oxygen isotope stage (MIS) 5–3, culminating in the 22–17 ka before present lowstand [Simms et al., 2007]. A prominent surface of erosion, the MIS 2 Sequence Boundary, demarcates the base of the valley and extends seaward across the continental shelf [Simms et al., 2007]. At the modern coastline, the valley is approximately 30–40 m deep, although much of this relief has been infilled with sediment. The terraced cross-sectional profile likely reflects the episodic nature of sea-level fall during the regression event

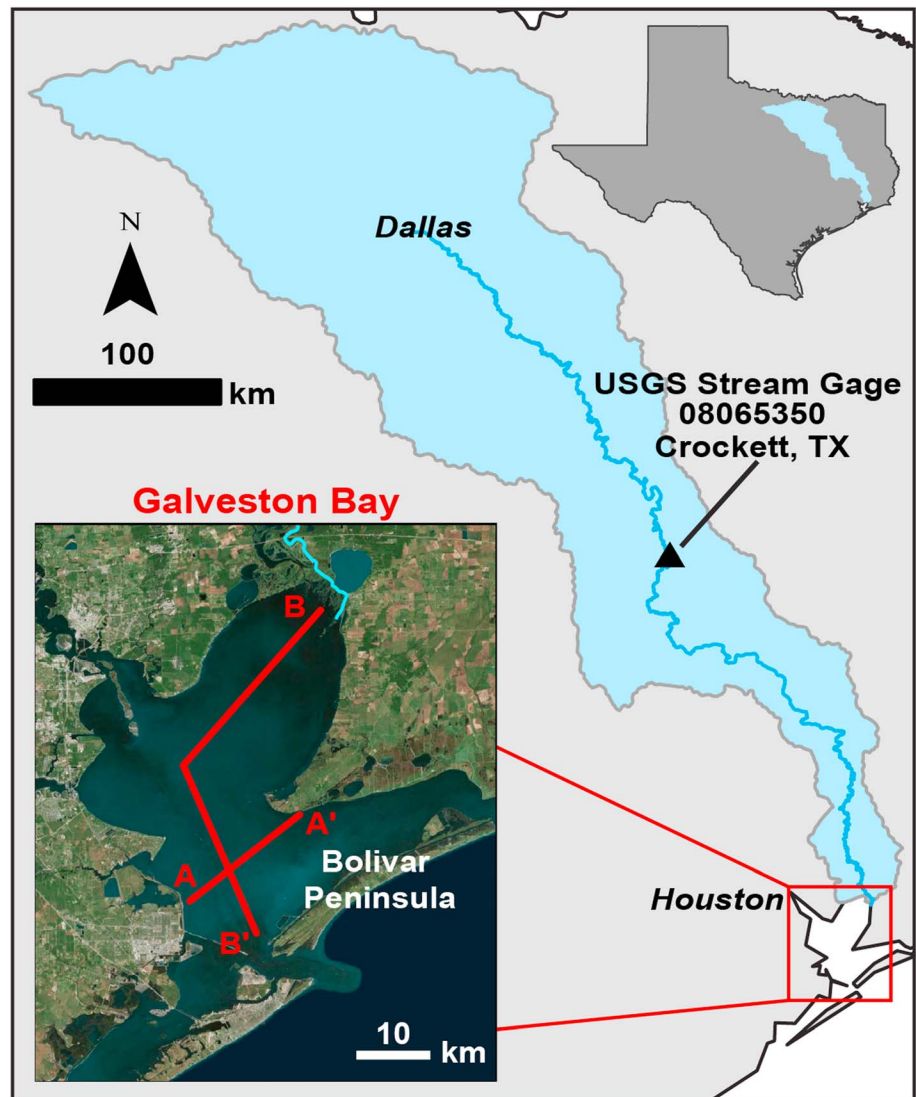


Figure 1. The Trinity River basin, which is approximately $44,000 \text{ km}^2$, maintains an average annual water discharge of $730 \text{ m}^3 \text{ s}^{-1}$ and an average annual sediment discharge of $6.2 \times 10^6 \text{ t}$. The average gradient is 1.6×10^{-4} [Rehkemper *et al.*, 1969; Anderson *et al.*, 2004]. A USGS stream gage station is located at Crockett, TX, where the Trinity River discharges, is enlarged in the inset. The locations for cross sections in Figures 2 and 3 are denoted as A-A' and B-B', respectively.

(Figure 2) [Rodriguez *et al.*, 2005]. Subsequently, the Trinity system responded to MIS 2 Holocene sea-level rise by aggrading and infilling its valley, beginning around 17 ka before present [Anderson *et al.*, 2008], when the rate of sea-level rise was approximately 10 mm yr^{-1} [Bard *et al.*, 1996]. A rapid transition from fluvial to bayhead delta sedimentation indicates a conspicuous response to base-level rise (Figure 3) [Anderson *et al.*, 2008].

The Trinity incised valley system is considered underfilled, based on the existence of Galveston Bay, and because of the exposure of Deweyville (Pleistocene-age) terraces that contain the modern Trinity River alluvial valley upstream of Galveston Bay (Figure 1) [Failing, 1969; Anderson *et al.*, 1992; Thomas and Anderson, 1994; Blum *et al.*, 1995; Simms *et al.*, 2006]. The underfilled character implies that sediment accumulation is unable to keep pace with the rate of accommodation produced via base-level rise [Simms *et al.*, 2006]. As has been recognized by previous researchers, antecedent topography of the incised valley, for example, floodplain width, exerts an influence on subsequent sedimentation patterns, and because the morphology of the Trinity valley is known, it is possible to explore its influence on fluvial-deltaic stratigraphy associated with infill (Figures 2 and 3) [Rodriguez *et al.*, 2005; Simms *et al.*, 2006; Anderson *et al.*, 2008].

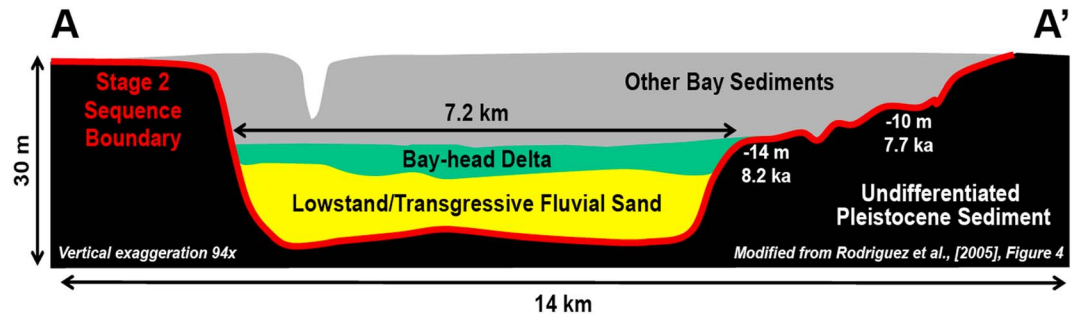


Figure 2. Cross-sectional interpretation of facies and valley morphology derived from seismic data and cores collected within Galveston Bay (see Figure 1 for location). The base of the valley is represented by a MIS 2 Sequence Boundary that formed during the last sea level lowstand. Radiocarbon dating of sediments within Galveston Bay is used to constrain the timing of sediment deposition. The valley began filling approximately 17 ka before present due to the onset of Holocene transgression. Increasing base-level-produced backstepping of coastal facies (figure modified from Rodriguez et al. [2005, Figure 4]).

2.2. Sea-Level and Associated Base-Level Rise

Sea-level rise and subsidence rates are well constrained for the northern Gulf of Mexico over the last 10,000 years. The values for these two parameters are considered cumulatively in order to estimate the base-level rise experienced by the Trinity system (i.e., base-level rise equals the combined effect of sea-level rise and subsidence). Milliken et al. [2008] produced a sea-level curve for the northern Gulf of Mexico derived from bayline peat and swash-zone deposits, which are reliable sea level markers and are easily datable (Figure 4) [Milliken et al., 2008]. Between approximately 10 and 8 ka before present, the time period of interest for this study, sea-level rise rates were $4.2 \pm 0.6 \text{ mm yr}^{-1}$ [Milliken et al., 2008]. Simms et al. [2013] reported that the long-term subsidence along the Texas Gulf Coast, primarily attributed to sediment loading, compaction, and isostatic adjustment, is approximately $0.07 \pm 0.03 \text{ mm yr}^{-1}$. Locally, however, subsidence rates could be as high as 3 mm yr^{-1} due to greater sedimentation and therefore enhanced compaction [Simms et al., 2013]. Summing sea-level rise and subsidence rates reported for 10–8 ka before present produces a base-level rise value of 4.3 mm yr^{-1} , which is within the bounds of variability for the reported sea-level rise and subsidence rates and is assumed to account for Glacial Isostatic Adjustment. While we use a single, standard rate of base-level rise (4.3 mm yr^{-1}) to simulate Holocene transgression, it is nevertheless possible to evaluate higher or lower rates within the modeling framework, thereby considering spatiotemporal adjustments.

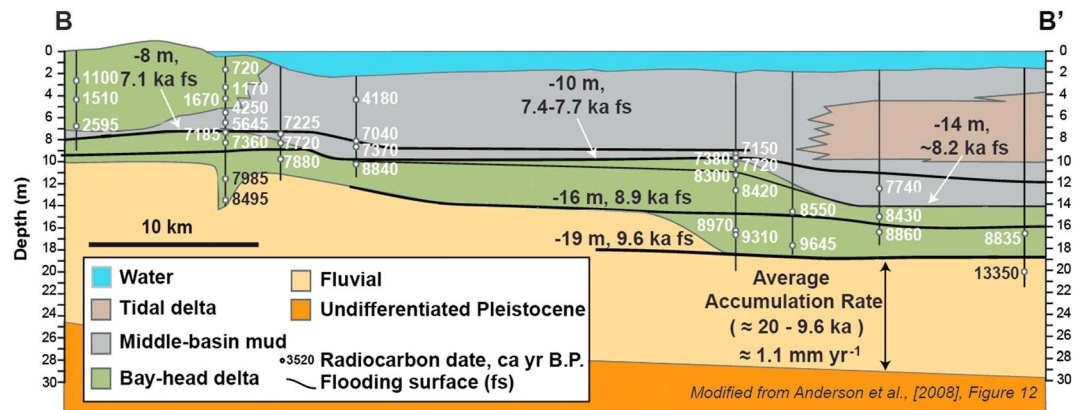


Figure 3. Axial dip section through Galveston Bay, interpreted from seismic and drill core data (see Figure 1 for location). Core locations, radiocarbon dates, and depositional facies are shown. Note how the facies backstep from south to north through time. Vertical aggradation rates of the fluvial facies are estimated to be 1.1 mm yr^{-1} (figure modified from Anderson et al. [2008, Figure 12]).

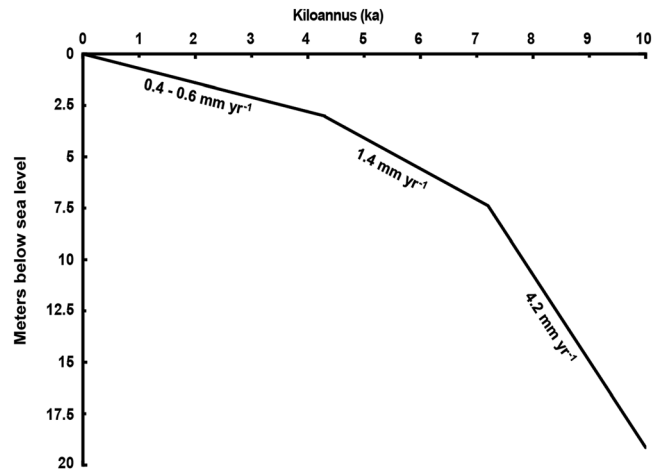


Figure 4. Northern Gulf of Mexico composite sea-level curve for 10 ka before present to present. Sea level was derived from bayline peat and swash zone deposits [Milliken *et al.*, 2008]. Our model simulates sea-level rise between 10 and 8 ka before present, when the average rate of rise was $4.2 \pm 0.6 \text{ mm yr}^{-1}$ (figure modified from Milliken *et al.* [2008]).

2.3. Water Discharge

Modern water discharge measurements for the Trinity River are used in this study because climate for the basin is estimated to have been consistent for much of the Holocene [Musgrove *et al.*, 2001; Weight *et al.*, 2011]. Water discharge measurements for the Trinity River are available from the U.S. Geological Survey (USGS) stream gage station 8065350 near Crockett, TX, located 380 river kilometers upstream of Galveston Bay (Figure 1). This station has been in operation from 1964 to present and was selected because it is the farthest downstream stream gage along the Trinity River that is not influenced by tides or backwater effects and because this station has produced continuous data of water stage and discharge.

The water discharge for a modern bankfull condition is considered in the model framework, assuming that the majority of stratigraphy-building sediment transport events occur during bankfull flow [Wolman and Miller, 1960]. This value is determined by comparing stage heights and the corresponding water discharges at Crockett, Texas, whereby bankfull discharge is the value above which no significant change in stage is measured [Leopold *et al.*, 1964]. For the Trinity River at Crockett, a range of values best characterizes this criterion, measuring $900\text{--}2,500 \text{ m}^3 \text{ s}^{-1}$. Within the model framework, flow does not emerge overbank, and therefore, the modeled flood conditions reflect flow within the prescribed channel. It is assumed that the base-level rise rate is low enough over centuries to millennia that as the modeled fluvial system evolves, it is able to morphodynamically equilibrate to the imposed changing boundary conditions and therefore maintain a geometry that contains bankfull discharge. A characteristic intermittency value of 0.05 or 20 d yr^{-1} is used, based on the distribution of flow events that fall within the bankfull conditions. It is emphasized that within the modeling framework, both bankfull flow and intermittency are readily adjustable.

Approximately 50 km below the Livingston Dam, the lower Trinity River achieves transport capacity of sand, possesses extensive point bars, and migrates laterally; this stretch of the lower Trinity River above the backwater zone is not influenced by the Livingston Dam and is used to inform our channel parameterization [Smith, 2012]. Channel width for the Trinity at bankfull conditions (B) is relatively constant throughout the lower few hundred kilometers of the basin, measuring approximately 200 m [Smith, 2012]. Although channel characteristics vary along the river, for simplicity we assume constant values of bankfull channel width, floodplain width, grain size, and water discharge, based on values that have been reported for the study area (Table 1) [Rehkemper *et al.*, 1969; Rodriguez *et al.*, 2005; Smith, 2012].

2.4. Floodplain Development

For the conditions of a constant elevation of the receiving basin (i.e., zero values of subsidence and sea-level rise), and reach-average sediment transport continuity, it is expected that sediment eroded from and deposited on the floodplain—that is, sediment exchange between the river channel and floodplain—occurs in equilibrium. Based on these considerations, previous morphodynamic models evaluating backwater

Table 1. Model Input Parameter Values

Variable	Definition	Value	Reference
B	Bankfull channel width	200 m	Smith [2012]
B_f	Floodplain width	7,200 m	Rodriguez et al. [2005]
C_f	Friction coefficient	3.6×10^{-3}	Parker [2004]
D	Median grain diameter	250 μm	Rehkemper et al. [1969]
g	Acceleration due to gravity	9.81 m s^{-2}	—
i	Intermittency parameter	0.05	Wolman and Miller [1960]
R	Submerged specific gravity of sediment	1.65	—
S	Channel bed slope	1.6×10^{-4} (initial slope)	Rehkemper et al. [1969]
λ_p	Bed porosity	0.4	Parker [2004]
ρ	Water density	1000 kg m^{-3}	—
Ω	Sinuosity	1.86	(Measured using Google Earth imagery of the Trinity River)

hydrodynamics have ignored exchange of channel and floodplain sediment [Parker, 2004; Chatanantavet et al., 2012; Lamb et al., 2012; Nittrouer et al., 2012; Ganti et al., 2014]. However, when considering system response to varying elevation of the receiving basin (i.e., base-level rise) over century to millennial time scales, it could be necessary to account for sediment exchange between the floodplain and channel [Parker et al., 2008b] because, over this time scale, base-level rise and increased accommodation space cause system aggradation and disequilibrium exchange between the channel and floodplain. Aggrading sediment buries previous deposits below the morphodynamic reworking depth of the system (typically characterized by the channel depth), thereby permanently sequestering this sediment as part of the floodplain stratigraphy [Straub et al., 2009; Straub and Esposito, 2013; Li et al., 2016].

Lauer and Parker [2008a, 2008b] calculated the characteristic advection length of mud on the floodplain for the Clark Fork River, Montana. The slow settling velocity of this sediment rendered the advection distance long: approximately 200 km. For the lower Trinity River floodplain, the valley width is significantly shorter ($B_f=7.2$ km) than the Lauer and Parker [2008a, 2008b] advection length because the Trinity system, as described above, is bounded by Pleistocene terraces. Therefore, it is possible that when the Trinity River floods, the valley fills with sediment-laden water that drains downstream, resulting in limited mud deposition. This process could be what accounts for the composition of Trinity floodplain sediments: sand with comparatively little mud [Phillips et al., 2004], as well as the sandy nature of the incised valley fill deposits [Rodriguez et al., 2005]. Additionally, any washload sediment that is deposited on the floodplain via overbank flows is likely subsequently eroded during lateral migration of the channel, whereby mud is entrained and transported downstream, and sandy channel bed sediment captured in point bars remains as part of the floodplain deposit [Parker et al., 2008a, 2008b, 2011].

2.5. Avulsions

Channel avulsions influence sediment partitioning and stratigraphy of fluvial-deltaic systems [Aslan and Blum, 1999; Mohrig et al., 2000; Slingerland and Smith, 2004; Hoyal and Sheets, 2009]. Channel avulsions are “set up” by sediment deposits aggrading the river bed, a process that tends to raise the elevation of the river surface and facilitate an avulsion “trigger,” which typically arises during flood events when levees are breached as a result of the reduced channel capacity that is unable to maintain water throughput [Slingerland and Smith, 2004]. The characteristic time to an avulsion (T_A) is estimated by $T_A = \frac{H}{V_A}$, where H is flow depth during bankfull conditions and V_A is the vertical rate of sediment aggradation of the channel bed [Mohrig et al., 2000; Jerolmack and Mohrig, 2007]. However, it is observed that in modern and paleo-systems alike, channels tend to avulse before the prescribed T_A [Mohrig et al., 2000; Jerolmack, 2009; Ganti et al., 2014]. For example, Ganti et al. [2014] showed that for the Yellow River, China, channel avulsion time scales are better approximated by using a modified depth of 0.3–0.6 H .

For fluvial-deltaic systems, avulsions typically occur near the backwater transition, because here downstream flow velocity decelerates (i.e., nonuniform flow typical of backwater regions), sediment transport capacity is reduced, and a region of focused deposition arises [Jerolmack and Swenson, 2007; Hoyal and Sheets, 2009; Chatanantavet et al., 2012; Lamb et al., 2012; Nittrouer et al., 2012]. This process tends to enhance V_A and therefore reduce T_A [Jerolmack and Swenson, 2007; Chatanantavet et al., 2012; Nittrouer et al., 2012].

3. Modeling Framework

A 1-D morphodynamic model is implemented to evaluate how changing rates of base-level rise and varying water discharge influences sediment deposition; input parameters applied within the model are defined in Table 1 and the *Notation* section. Accounting for sea-level rise in a morphodynamic model has been described previously [Parker *et al.*, 2008a, 2008b]; however, applying the concepts of base-level rise and channel-floodplain interaction to evaluate changes in sediment deposition patterns to the channel bed, and then linking this to the spatiotemporal conditions of channel avulsions, has not yet been explored. An additional aim of the modeling framework is to evaluate the capacity for backwater hydrodynamics, over time scales of centuries to millennia, to produce focused sedimentation that infills the incised Trinity River valley during the latest Holocene transgression.

In order to assess hydrodynamics, our model evaluates flow depth (H) during bankfull conditions through along-stream distance (x):

$$\frac{dH}{dx} = \frac{S - C_f Fr^2}{1 - Fr^2} \quad (1)$$

where S is the channel bed slope, C_f is a constant friction coefficient, and Fr is the Froude number, determined by $Fr = U(gH)^{-0.5}$, where g is the acceleration due to gravity and U is the reach-average flow velocity (Table 1). Equation (1) is solved by using a predictor-corrector scheme, where the initial linear bed slope is defined. This initial value is set to 1.6×10^{-4} , which characterizes the lower Trinity River water surface and floodplain (Table 1) [Rehkemper *et al.*, 1969]. The channel bed slope is then allowed to evolve and is iteratively calculated between model cells, as sediment enters and is eroded from or deposited on the modeled system. The spatial step is equal to 1 km, and the time step is equal to 1 year; both the space and time steps in the modeling framework are sufficient to evolve and link morphodynamics to the production of fluvial-deltaic stratigraphy over the domain of interest: several hundred kilometers and many centuries to millennia.

In order to account for sea-level rise, we define flow depth at the downstream most cell as follows:

$$\zeta_d = \zeta_{do} + \zeta t \quad (2)$$

where ζ_d is the water surface elevation at the downstream end of the modeled domain, ζ_{do} is the initial water surface elevation prior to model calculations, and ζ is the rate of base-level rise. In this way, we can evaluate the water depth at the downstream cell as $H(x=0) = H_o + \zeta t$, where H_o is the initial water depth (i.e., $H_o = H(t=0) = 10$ m) and ζ is the sea-level rise rate. We apply a constant rate of base-level rise ($\zeta = 4.3 \text{ mm yr}^{-1}$) over the duration of the model run. The backwater length—the length of nonuniform flow—is evaluated based on the distance between the upstream and downstream points where the water surface slope approaches zero. Upstream of the backwater region, uniform flow velocity exists where the channel bed and water surface profiles are parallel, i.e., $(dH/dx = 0)$. We define the upstream initiation of backwater to start at $dH/dx > 5 \times 10^{-6}$, a threshold that is considerably less than the initial slope of the uniform channel bed (i.e., $5 \times 10^{-6} \ll 1.6 \times 10^{-4}$), and which coincides with the location where flow velocity begins to diminish. Backwater effects extend downstream to the receiving basin, and the downstream point of termination of this affected zone is defined by the location where the water surface slope drops below the threshold value of $dh/dx < 5 \times 10^{-6}$, where $h = H + \eta$ is the bankfull water surface elevation referenced to a fixed datum below the bed (η).

Sediment flux per-unit-channel width ($q_b, q_t = \sqrt{RgDD} \frac{0.05}{C_r} \left(\frac{\tau_b}{\rho RgD} \right)^{2.5}$, where R is the submerged specific gravity of sediment, D is the median grain diameter, and ρ is the water density) is determined by using the Engelund and Hansen [1967] total load equation for bed material, which is considered the “formative” sediment of lowland river morphodynamics [Parker, 2004]. τ_b is the boundary shear stress and determined by $\tau_b = \rho C_f U^2$. A constant rate of sediment input ($Q_s = 0.12 \text{ m}^3 \text{ s}^{-1}$ [Rehkemper *et al.*, 1969]) is applied to the upstream most cell in the model, adjusted for channel width to calculate q_b , and allowed to reach transport capacity over 200 km before entering the lowermost 300 km reach of interest evaluated here. Additionally, sediment input is subjected to the intermittency of flood flows. See Table 1 for model input parameter values.

A spatial divergence in sediment flux for each spatiotemporal step ($\partial q_b / \partial x$) is calculated, and these values are used to determine the resulting change in-channel bed elevation ($\partial \eta / \partial t$) based on a simplified version of the Exner equation [Paola and Voller, 2005]. An intermittency parameter (i) is applied to the simple Exner equation because the fluvial system is considered only morphologically active for a fraction of the modeled time:

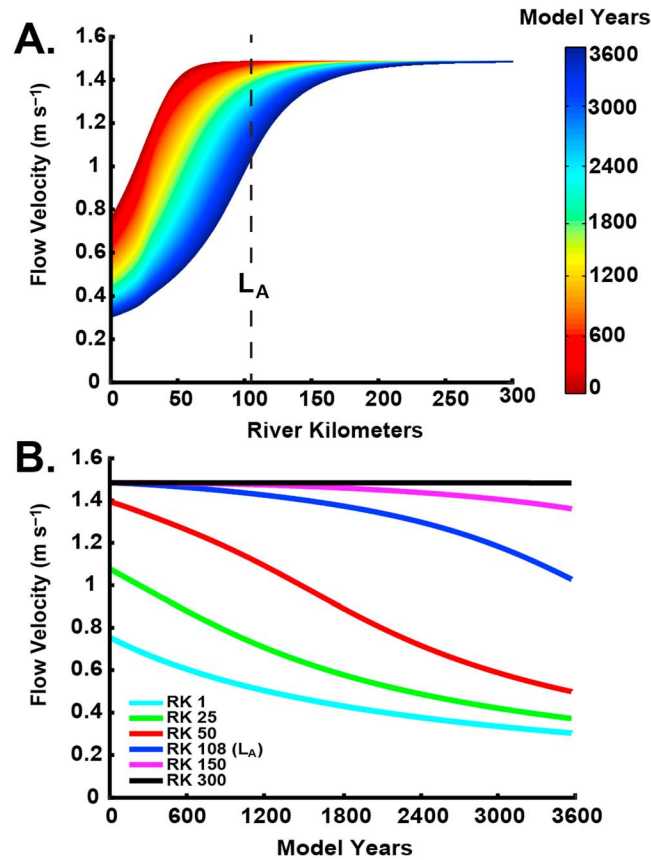


Figure 5. (a) Spatiotemporal flow velocity, plotted from the onset of the model (0 model years) to the time for an avulsion ($T_A = 3,548$ model years). The avulsion location (L_A) is shown by the dashed line, at river kilometer (RK) 108. (b) Flow velocity and time (model years) shown for denoted locations along stream, where RK represents river kilometers upstream of the outlet. Flow velocity decreases downstream and with increasing model time due to increasing flow depth associated with base-level rise through time (equations (1) and (2)). Water discharge ($Q_w = 1,500 \text{ m}^3 \text{ s}^{-1}$), sediment input ($Q_s = 0.12 \text{ m}^3 \text{ s}^{-1}$), and rate of base-level rise (4.3 mm yr^{-1}) are held constant, and the time and location of avulsion are based on an avulsion threshold of $0.3H$ in Figures 5a and 5b.

of channel bed aggradation, due to sediment partitioning between the channel and the floodplain as a result of lateral mobility of the channel across its floodplain combined with changing base level conditions [Parker et al., 2008a, 2008b]. As will be discussed below, this modified version of the Exner equation captures the system dynamics over centennial to millennial time scales, i.e., significantly longer than previous studies replicating sediment transport interactions influenced by backwater hydrodynamics. Equation (4) is solved numerically by using central differences for time computations and a predictor-corrector scheme for spatial computations; the Euler method is employed to calculate q_t in the corrector phase. We define the vertical aggradation rate of the channel for a given location, x , as $V_A = \partial\eta(x)/\partial t$.

Within the modeling framework, channel sedimentation is considered over the time period to an avulsion event, by assuming that this avulsion set up time represents the characteristic “life cycle” of a fluvial-deltaic distributary channel [e.g., Viparelli et al., 2015]. An avulsion is considered to occur in the model domain where the channel bed aggrades (η ; equation (4)) to a designated fraction of the flow depth (H ; equation (1)). Specifically, a range of $0.3\text{--}0.6H$ is considered as suggested by Ganti et al. [2014]. Only the time leading to an avulsion event is modeled; the avulsion process itself, e.g., the trigger that leads to the channel changing its path over the floodplain, is not considered here. For each time step, flow depth is computed based on the calculated bed elevation change (η ; equation (4)). Since the downstream-most boundary changes with time

$$(1 - \lambda_p) \frac{\partial \eta}{\partial t} = \frac{-\partial q_t}{\partial x} \quad (3)$$

where λ_p is bed porosity (Table 1). Equation (3) captures bed elevation change for the modeled domain and represents a simple channel model whereby all sediment remains within the channel.

Herein, a modified version of equation (3) is considered, whereby bank-full channel width (B), channel sinuosity (Ω), and floodplain width (B_f) are introduced to modify the rate of channel bed aggradation, and thus account for sediment partitioning between the channel and adjacent floodplain [Parker et al., 2008a, 2008b]:

$$(1 - \lambda_p) \frac{\partial \eta}{\partial t} = -\Omega \frac{B}{B_f} \frac{\partial q_t}{\partial x} \quad (4)$$

Sinuosity is measured based on the modern Trinity River ($\Omega = 1.86$; Table 1), and this value is typical for lowland, meandering river channels [Parker, 2004; Parker et al., 2008a, 2008b]. Equation (4) serves to partition sediment between the channel and floodplain and represents a coupled channel-floodplain model over the spatiotemporal scales considered here [Parker et al., 2008a, 2008b]. It is emphasized that this formulation does not explicitly model the processes of floodplain sedimentation, but instead serves as a means to evaluate a modified rate

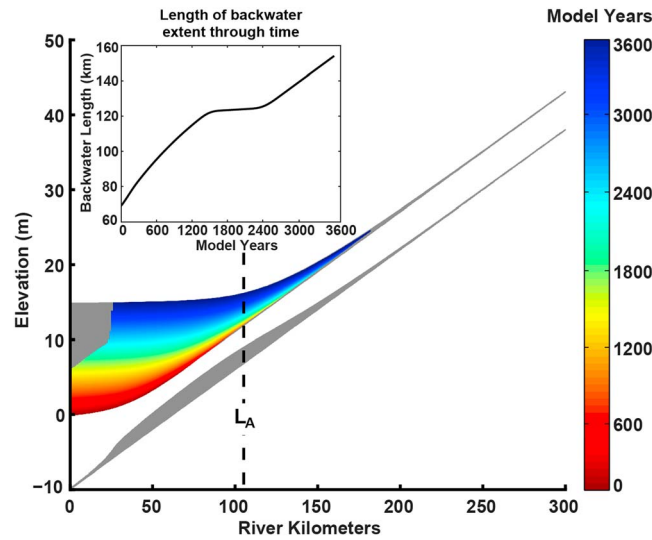


Figure 6. Backwater influence on the water surface profile, with respect to time (model years). Water discharge ($Q_w = 1,500 \text{ m}^3 \text{ s}^{-1}$), sediment input ($Q_s = 0.12 \text{ m}^3 \text{ s}^{-1}$), and rate of base-level rise (4.3 mm yr^{-1}) are held constant, and the time and location of avulsion are based on an avulsion threshold of $0.3H$. The gray regions of the water surface denote where the water surface is not contained within the backwater region (i.e., regions that exhibit $dh/dx > 5 \times 10^{-6}$ (upstream) and $dh/dx < 5 \times 10^{-6}$ (downstream) where $h = H + \eta$). Note how the backwater region migrates upstream through time, associated with increasing base level. The gray regions on the channel bed represent sediment deposited prior to reaching the avulsion threshold. The black dashed line represents the avulsion location (L_A), occurring at 108 RK after 3,548 model years. Inset: Plot of backwater length and time (model years; see text for details on backwater length calculation); note how the length of the backwater region increases over time.

of backwater lengthens over time. It follows then that the spatial decrease in flow velocity, shear stress, and sediment flux should also migrate upstream over time (Figures 5 and 7). These conditions combine to produce upstream movement of the avulsion location as a function of base-level rise. For example, Figures 8a–8c and 8g, which represent individual model runs with differing rates of base-level rise which were held constant, show that avulsions occur in positions progressively farther upstream with increasing rates of base-level rise.

Characteristic Holocene base-level rise ranges from 3.7 to 4.8 mm yr^{-1} based on reported values [Milliken *et al.*, 2008; Simms *et al.*, 2013] discussed in section 2.2; since time and location of avulsion vary with base-level rise rate, a range of times and locations best represents the results of our model. A base-level rise rate of 3.7 mm yr^{-1} produces a time and location of avulsion of 2,548 model years and 71 river kilometers, respectively, while a base-level rise rate of 4.8 mm yr^{-1} does not produce an avulsion due to base-level rise outpacing in-channel sedimentation. Herein, we discuss the results of our model by using a constant base-level rise rate of 4.3 mm yr^{-1} , unless otherwise specified.

4.1. Flow Velocity, Sediment Transport, and Sediment Deposition Patterns

The model results are bounded by base-level rise and as such the model captures variability of flow velocity in space and time (Figure 5). Flow velocity profiles maintain a similar trend through time (Figure 5a) but at any given spatial point, identified as river kilometer (RK) upstream of the outlet, flow velocity decreases over time (Figure 5b). This is possible because while water discharge and channel width are held constant, cross-sectional area increases via increasing flow depth in the downstream direction due to base-level rise, assuming that the aggradation of sediment atop the levees keeps pace with base-level rise. It is noted that for a given water discharge, flow depth only increases in the backwater region of the channel due to base-level rise; upstream of backwater influence (i.e., in the normal flow regime) flow depth is uniform. Additionally, flow velocity decreases

(equation (2)), flow depth must be calculated iteratively at each time step within the model to identify the location where the channel aggrades to the imposed avulsion threshold.

4. Results

Within the backwater region of the river the water surface profile is influenced by the elevation of the receiving basin and base-level rise over time, which therefore affects the upstream extent of backwater conditions. As a result of the imposed base-level rise, changes in flow depth (H) are more significant in the downstream backwater-influenced portion of the model than in the upstream normal flow reach. Channel cross-sectional area ($A = B * H$) is therefore greater downstream than upstream. Following $U = \frac{Q_w}{A}$, where Q_w is bankfull water discharge, there is a downstream decrease in flow velocity, as can be seen in Figure 5. As base-level increases, the onset and termination of the backwater region backstep through time, rendering the backwater region mobile (Figure 6). Furthermore, the measured extent

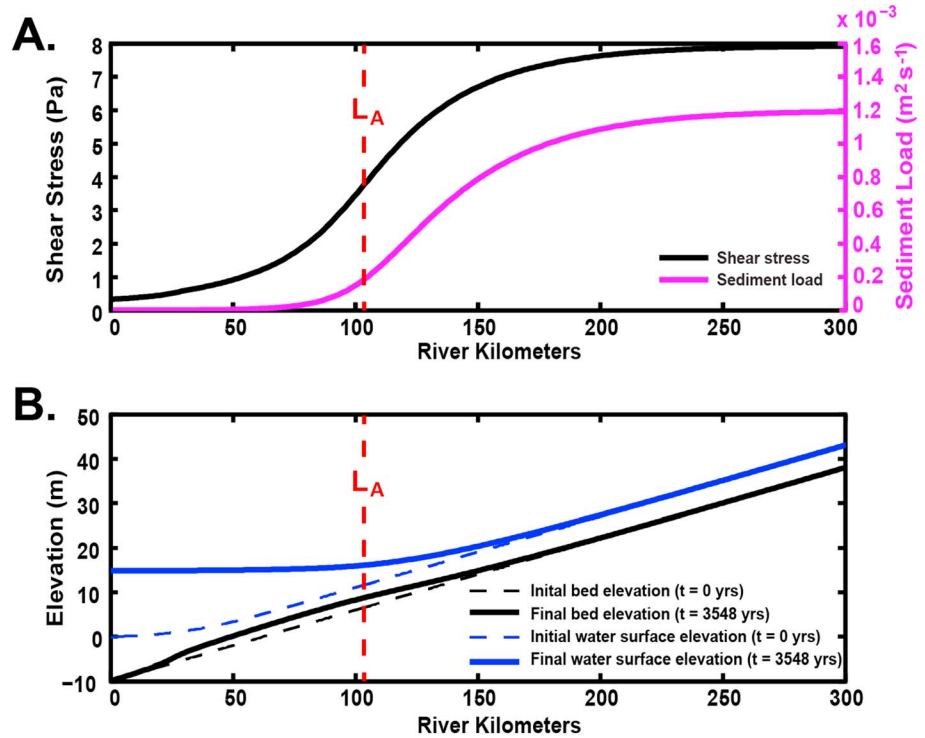


Figure 7. (a) Shear stress (τ_b ; black line, left y axis) and sediment load (q_t ; magenta line, right y axis), plotted with river kilometers upstream of the outlet. The location of avulsion is denoted by a red dashed line ($L_A = 108$ RK). (b) Bed elevation profile (solid and dashed black lines) and water surface elevation profile (solid and dashed blue lines) plotted over space for the initial (dashed lines) and final time (i.e., avulsion time; solid lines; $T_A = 3,548$ model years), for a base-level rise rate of 4.3 mm yr^{-1} . Water discharge ($Q_w = 1,500 \text{ m}^3 \text{ s}^{-1}$), sediment input ($Q_s = 0.12 \text{ m}^3 \text{ s}^{-1}$), and rate of base-level rise (4.3 mm yr^{-1}) are held constant, and the time and location of avulsion are based on an avulsion threshold of $0.3H$ in Figures 7a and 7b.

downstream for each time step, and the location for the onset of decreasing flow velocity migrates upstream over time (Figure 5). For example, in Figure 5a a flow velocity of 1.3 m s^{-1} occurs at 41 RK at time 0, and after $\sim 3,500$ model years, the same flow velocity coincides with 138 RK. As seen in Figure 5a, flow velocity decreases considerably, as is expressed by the steeply sloping region for the plot of flow velocity through time and space. A constant flow velocity is observed in the upstream portion of the model and is indicative of normal (uniform) flow conditions; indeed, all flow velocity profiles converge to normal flow conditions in the upstream model domain, even though the extent of uniform flow and the transition to nonuniform flow migrate upstream over time.

Flow velocity (U ; Figure 5) is used to calculate boundary shear stress (τ_b ; Figure 7a, black line) and sediment transport (q_t ; Figure 7a, magenta line). Bed material transport capacity is a strongly nonlinear function of flow velocity as seen in Figure 7a. The avulsion location ($L_A = 108$ RK) coincides with the regions of greatest spatial change for shear stress and sediment load (Figure 7a). As seen in Figure 7b, the region of channel bed sediment deposition coincides with the region of rapid spatial decrease in shear stress and sediment transport rates. In other words, the majority of sediment deposited on the channel bed occurs within the region of greatest decreasing transport capacity. Additionally, based on mass balance calculations, it is determined that a minor amount of sediment exits the model domain, as indicated by the near-zero sediment discharge values at the outlet (Figure 7a). This nominal sediment volume does not change the overall model results.

The sensitivity of the model is tested by varying base-level rise rates, and the findings show that the morphology of the sediment deposit on the channel bed is transient and varies in accordance with base-level rise. Figures 8a–8e depict five scenarios of changing rates of base-level rise to portray the possible morphologies of sediment deposits evolving up to an avulsion threshold of $0.3H$. Under the static boundary condition of

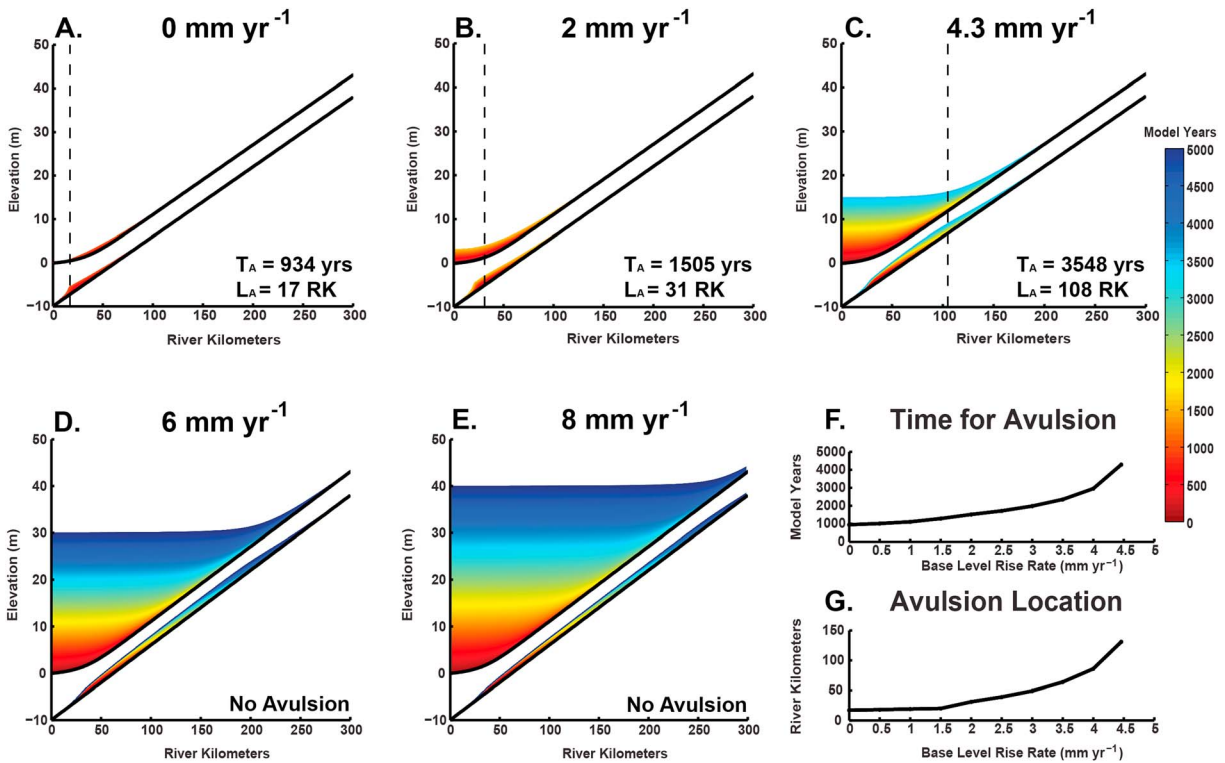


Figure 8. Five model runs (refer to Table 1) selected to portray the effects of the rate of base-level rise on sediment wedge morphology, the time to avulsion (T_A), and the avulsion location (L_A). The upper curves are the water surface, while the lower curves represent sediment deposited on the channel bed. The dashed black lines represent the avulsion location in cases where avulsions occur. Water discharge ($Q_w = 1,500 \text{ m}^3 \text{ s}^{-1}$) and sediment input ($Q_s = 0.12 \text{ m}^3 \text{ s}^{-1}$) are held constant for all runs; the time to avulsion is based on an avulsion threshold of $0.3H$. (a) No base-level rise, (b) 2 mm yr^{-1} , (c) 4.3 mm yr^{-1} , (d) 6 mm yr^{-1} , (e) 8 mm yr^{-1} , and (f) time to avulsion (T_A) plotted for various base-level rise rates. (g) Avulsion location (L_A) plotted for various base-level rise rates. Note that avulsions do not occur at base-level rise rates greater than 4.5 mm yr^{-1} for the water and sediment discharge conditions considered.

zero base-level rise ($\zeta = 0 \text{ mm yr}^{-1}$; Figure 8a), the sediment deposit “wedge” simply progrades downstream. Similarly, the sediment wedge produced for a base-level rise rate of 2 mm yr^{-1} progrades downstream, although a greater bed elevation (thicker deposit) arises compared to the static scenario, because of the increased time to reach the avulsion threshold (Figure 8b). When base-level rise is simulated at 4.3 mm yr^{-1} (the value consistent with base-level rise experienced by the Trinity River during the early to middle Holocene), the sediment wedge first progrades, then backsteps before reaching the avulsion threshold (Figure 8c). For rates greater than 5 mm yr^{-1} , the sediment wedge progrades, then retrogrades but never aggrades to the avulsion threshold (Figures 8d and 8e). As the base-level rise rate progresses from a static scenario (zero), the deposited sediment wedge extends over a greater distance.

The influence of base-level rise is also reflected by the morphology of the sediment deposited on the channel bed. It is clear that in all scenarios depicted in Figures 8a–8e, the slope of the water surface profile mimics the profile of the sediment wedge. Parker [2004] developed a model with static boundary conditions whereby sediment is deposited within in the backwater region, re-grading the downstream bed slope and producing normal flow conditions. Our model results show that sediment is also deposited on the bed in a backstepping fashion, which is especially pronounced for conditions of base-level rise rates greater than 2 mm yr^{-1} .

The locus of sediment deposition is tracked by determining the location of the maximum change in bed elevation between each time step ($\partial\eta/\partial t$); this location is sequentially plotted in Figure 9 to determine the rate at which progradation and backstepping occur within the channel. As the maximum change in bed elevation moves downstream, a negative slope is produced, as seen in Figure 9, representing a prograding sediment deposit. As the maximum change in bed elevation migrates upstream, a positive slope is produced, associated with the backstepping sediment deposition (Figure 9). For rates of base-level rise of 4.3 mm yr^{-1} ,

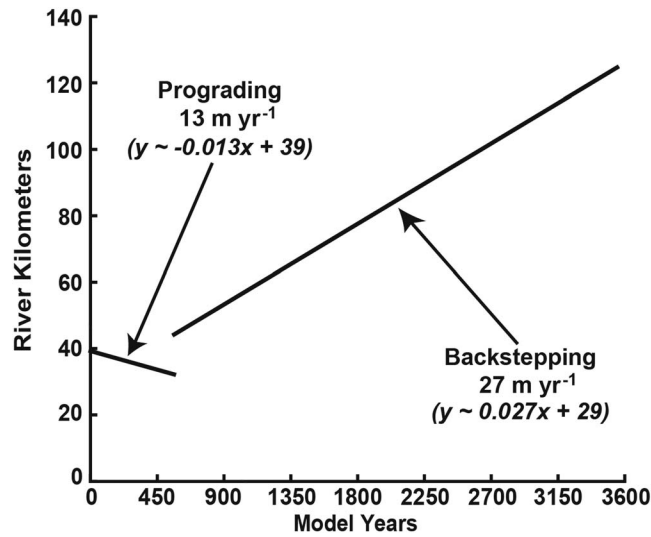


Figure 9. The location for the depositional front (river kilometers, referenced above the outlet), as calculated based on the maximum change in bed elevation, and time (model years). Note that periods of sediment progradation are indicated by a negative slope (i.e., advancing progradation front with time) and periods of sediment backstepping are indicated by a positive slope (i.e., retreating depositional front with time). The model considers the input parameters of the Trinity River with a base-level rise rate of 4.3 mm yr^{-1} and water discharge of $1,500 \text{ m}^3 \text{ s}^{-1}$ (see Table 1 for additional input parameters).

sediment progrades downstream at a rate of 13 m yr^{-1} and backsteps at a rate of 27 m yr^{-1} . This transition between prograding and backstepping sediment deposition for conditions reflecting Holocene transgression occurs after 564 model years and is depicted by the break in slope seen in Figure 9.

4.2. Sensitivity to Water and Sediment Discharge, Partitioning of Sediment to the Floodplain, and Avulsion Threshold

Our analysis shows that the time to avulsion varies with discharge and the rate of base-level rise. Specifically, Figure 10a demonstrates model sensitivity to the observed range of bankfull discharges ($900\text{--}2,500 \text{ m}^3 \text{ s}^{-1}$), assuming capacity transport at the beginning of each simulation. For a given discharge, time to avulsion increases with the rate of base-level

rise. Conversely, for a given base-level rise, time to avulsion decreases with greater discharge due to larger volumes of sediment in transport and thus greater deposition in the backwater zone. However, when rates of base-level rise outpace deposition, avulsion is precluded. In contrast to the above results, when floodplain sedimentation is neglected (equation (3)), time to avulsion is greatly reduced and is insensitive to both discharge and the rate of base-level rise (Figure 10b). The contrasting results of Figures 10a and 10b emphasize the importance of accounting for sediment partitioning between the channel and floodplain when considering avulsions over stratigraphically meaningful time scales. For example, the lowest avulsion threshold as

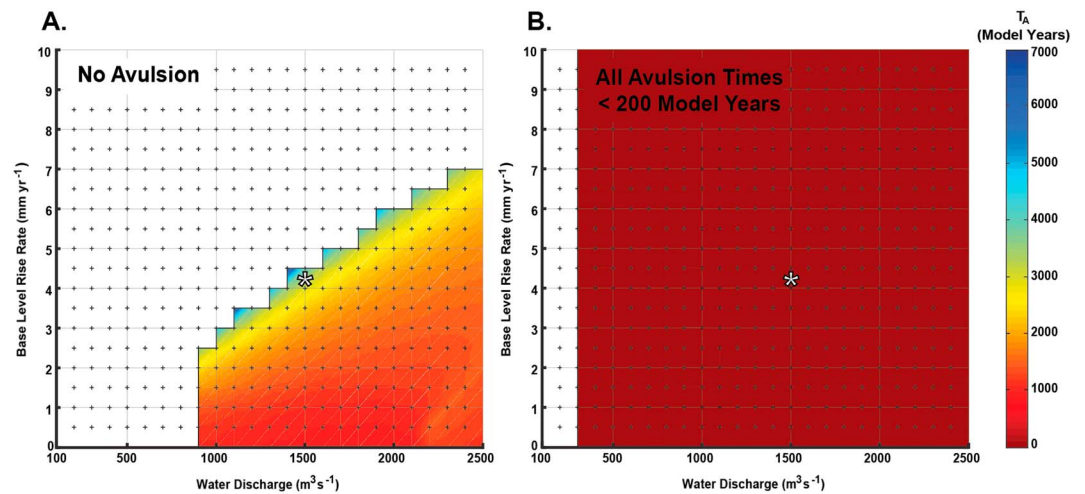


Figure 10. Phase diagrams showing time to avulsion for varying base-level rise rates and water discharge conditions. Avulsion threshold is held constant at $0.3H$ for both scenarios; see Table 1 for additional input parameters. The white asterisk represents modeled conditions of the early to middle Holocene Trinity River. (a) Time to avulsion utilizing a channel-floodplain model which partitions sediment to the floodplain (equation (4)). (b) Time to avulsion utilizing a simple channel model with no sediment partitioning to the floodplain (equation (3)).

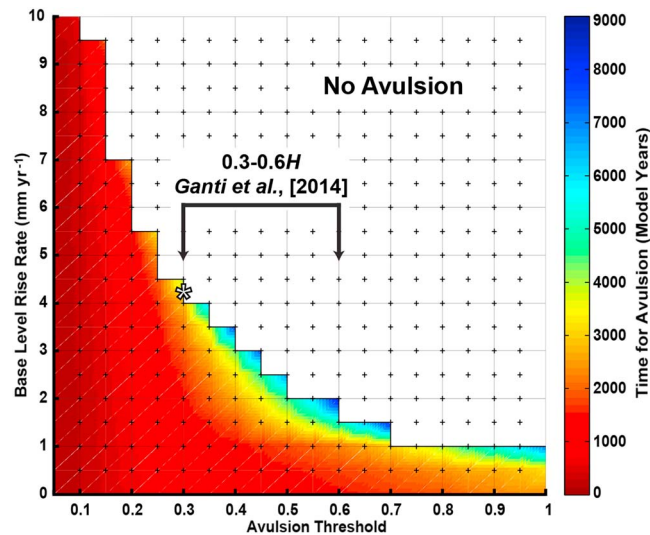


Figure 11. Phase diagram for the time to avulsion based on varying base-level rise rates and avulsion thresholds. The avulsion threshold is expressed as a fraction of the channel flow depth (H), and the time to avulsion (T_A) is based on when the sediment deposit aggrades to the avulsion threshold. Water discharge is held constant at $1500 \text{ m}^3 \text{ s}^{-1}$; see Table 1 for additional input parameters. The white asterisk represents modeled conditions of the early to middle Holocene Trinity River.

proposed by *Ganti et al.* [2014] ($0.3H$) generates no avulsions for base-level rise rates greater than 4.5 mm yr^{-1} , when using the channel-floodplain model (equation (4) and Figures 8f, 8g and 10a) and input parameters that characterize the Trinity River; however, utilizing the same avulsion threshold and a simple channel model (equation (3) and Figure 10b), avulsions are generated for base-level rise rates up to 10 mm yr^{-1} .

To explore model sensitivity to the avulsion threshold parameter, a range of values was examined ($0.05H$ - H) in $0.05H$ increments. Figure 11 shows how the time to avulsion varies as a function of both the avulsion threshold parameter and the rate of base-level rise for a constant water discharge ($Q_w = 1,500 \text{ m}^3 \text{ s}^{-1}$). As expected, the results show that more time is required to reach higher avulsion thresholds than for lower avulsion thresholds. Increasing the avulsion threshold decreases the highest rate of base-level rise under which an avulsion can be set up. If the rate of base-level rise exceeds the rate of sediment aggradation, the avulsion threshold is never met. For lower thresholds (e.g., $0.3H$), avulsions can occur despite high rates of base-level rise (up to 4.5 mm yr^{-1} ; Figure 11) because less sediment deposition is required to attain the threshold for avulsion. Conversely, for higher thresholds (e.g., $0.6H$), an avulsion is produced only for lower rates of base-level rise (less than 2 mm yr^{-1} ; Figure 11) because more sediment deposition is required to reach the avulsion threshold. Lower avulsion thresholds increase the potential for an avulsion, while higher avulsion thresholds decrease the potential for an avulsion at any rate of base-level rise. These results explain why the avulsion time for a $0.3H$ threshold at 4.5 mm yr^{-1} is less than the avulsion time for a $0.5H$ threshold at 2.5 mm yr^{-1} (Figure 11). Furthermore, the modeled system exhibited in Figure 11 is unable to infill its channel with sediment to an avulsion threshold at rates of base-level rise greater than 10 mm yr^{-1} due to the fact that base-level rise rate outpaces in-channel aggradation.

5. Discussion

Backwater morphodynamics produce sediment deposition within fluvial-deltaic channels, as has been shown in previous studies, and the net effect of this process is to set up channel avulsions whereby sediment infill reaches a threshold value, with respect to the overall channel depth [e.g., *Lamb et al.*, 2012; *Nittrouer et al.*, 2012; *Ganti et al.*, 2014]. We confirm that for the Trinity River, the avulsion location for a condition of fixed base-level rise remains within the backwater region ($L_A = 108 \text{ RK}$), and thus does not extend upstream into the region of uniform flow (Figure 6). The models of *Chatanantavet et al.* [2012] and *Lamb et al.* [2012] showed

that an M2 curve (spatially accelerating flow) and enhanced sediment transport capacity, resulting from the drawdown of the water surface profile toward the receiving basin during river floods, produce channel bed scour. Specifically, *Chatanantavet et al.* [2012] proposed that it is the alternation between both M1 and M2 conditions that facilitates avulsion setup. Interestingly, M2 conditions are not obtained for the Trinity River model, yet avulsion still occurs. The absence of M2 conditions predicted from the model is due to the fact that the simulated water discharge is sufficiently low, precluding a hydrodynamic drawdown effect at the river mouth. Our results therefore show that there is also a propensity for avulsions within the backwater reach without occurrence of alternating M1 and M2 conditions.

The differences in the results presented here and those of previous studies could be associated with the rising condition of base level and the associated response of channel bed sedimentation within the backwater region. The motivation here is to evaluate morphodynamic responses to these boundary conditions, in order to mimic a condition of transgression over stratigraphically meaningful time scales. The discussion below focuses on the specific case of the Trinity River system, where we find that by adding base-level rise as a boundary condition (equation (2)) to the model of backwater morphodynamics, the timing, location, and magnitude of sedimentation patterns, and therefore avulsion conditions, are influenced. This constitutes a new contribution provided by the analyses presented herein.

5.1. Trinity River Sedimentation Patterns During Transgression and Rates of Incised Valley Infill

Trinity River incised valley stratigraphy consists of fluvial, deltaic, and basin mud deposits, which are characterized by backstepping stratigraphic architecture that reflects the landward shift of these depositional environments due to sea-level rise or changes in valley morphology [Thomas and Anderson, 1994; Rodriguez et al., 2005; Anderson et al., 2008]. The deposits filled an incised valley, and therefore, much of the sediment mass is contained and relatively unaffected by transgressive ravinement. Importantly, researchers have identified backstepping of the sedimentary facies associated with a time period for when sea level was rising at an average rate of 4.2 mm yr^{-1} (Figures 2–4) [Anderson et al., 2008; Milliken et al., 2008], and this is consistent with the model results that demonstrate a backstepping character of in-channel sedimentation for rates of base-level rise greater than 2 mm yr^{-1} (Figure 6). However, it is also known that a significant facies backstepping event occurred between ~ 7.4 and ~ 7.7 ka before present, when the rate of sea-level rise (1.4 mm yr^{-1}) was significantly lower than early to middle Holocene rates, although this flooding event is recognized to have occurred when sea level reached the elevation of a broad, terraced portion of the valley, which allowed for a significantly increased area of inundation and sediment accommodation (Figures 2–4) [Rodriguez et al., 2005]. Therefore, backstepping of sedimentary facies within the Trinity incised valley system, as recorded in the stratigraphy, occurs due to the effects of sea-level rise rate and valley morphology.

In the absence of variable valley geometry, as modeled for the Trinity system, sedimentation patterns may either backstep or prograde depending on a “threshold” rate of base-level rise. This threshold for the Trinity River is determined to be 2 mm yr^{-1} ; for this rate of base-level rise, the frequency and location of channel avulsion are essentially fixed. For rates of base-level rise less than 2 mm yr^{-1} , the system progrades and aggrades contemporaneously, which over time leads to the development of normal flow conditions progressively downstream as the channel bed aggrades basinward, thereby countering backwater effects by maintaining uniform flow depth. This situation of the channel re-equilibrating and nullifying backwater conditions has been noted in models that do not consider base level adjustments [e.g., Parker, 2004]. Thus, for relatively small changes in base-level rise, the fluvial system maintains sufficient sediment volume to aggrade the bed and maintain uniform flow. Alternatively, for conditions of base-level rise greater than 2 mm yr^{-1} , sediment backstepping develops, whereby the region of greatest sediment deposition migrates upstream over time. This threshold base-level rise rate for the Trinity River system (2 mm yr^{-1}) could be applicable to other lowland fluvial systems that possess similar physical characteristics (slope, discharge, and sediment transport rate). In order to appropriately constrain the progradation and backstepping threshold conditions for a unique system, input parameters that characterize the fluvial system should be implemented into the modeling framework.

The backstepping of backwater-induced deposition modeled for the Trinity system is compared to measurements acquired via stratigraphy. The model results indicate that for a base-level rise of 4.3 mm yr^{-1} , the

region of focused deposition moves landward at a rate of 27 m yr^{-1} (Figure 9). This value closely corresponds to the observed backstepping measured from the fluvial-deltaic sedimentary facies within the incised valley deposits located in Galveston Bay, $\sim 25 \text{ m yr}^{-1}$ [Anderson *et al.*, 2008] (Figures 3 and 9). We propose that the backstepping rate of in-channel sedimentation during transgression of the Holocene Trinity system may be approximated by the quotient of base-level rise and the characteristic channel bed slope. For example, the Holocene Trinity River base-level rise used here (4.3 mm yr^{-1}) and characteristic channel slope of 1.6×10^{-4} produce an estimated rate of backstepping of 27 m yr^{-1} , which is a value consistent with both the measured and modeled results.

Vertical aggradation rates measured for the fluvial-deltaic sand of the Trinity incised valley deposits can also be compared to modeled results. Based on, first, the sediment thickness ($\sim 11.4 \text{ m}$) between the top of Pleistocene sediments (the onset of Galveston Bay sedimentation; $\sim 20 \text{ ka}$ before present) and a prominent flooding surface (9.6 ka before present) which represents cessation of channel sedimentation and onset of bay mud deposition, and second, the measured age difference between these two surfaces, the vertical rate of aggradation for the fluvial-deltaic sand facies is estimated as $\sim 1.1 \text{ mm yr}^{-1}$ [Rodriguez *et al.*, 2005; Anderson *et al.*, 2008] (Figure 3). The results of the channel sedimentation model presented herein constrain a vertical aggradation rate for this region to 0.68 mm yr^{-1} by considering the thickest sediment deposit divided by the time to avulsion. The discrepancy between the measured and modeled vertical aggradation rates could be due to the fact that the model considers backwater-induced sedimentation only within the fluvial dispersal channel, and not beyond the channel mouth. Therefore, the model neglects deposition associated with the downstream deltaic facies, thereby underpredicting the total sand deposited within the incised valley. Furthermore, measurements of sand deposit ages and thickness may not discriminate between the channel and downstream deltaic facies. Additionally, the difference could also be associated with variable, and/or poorly constrained, age control for the fluvial-deltaic sand deposits of Galveston Bay. It is nevertheless interesting that neither the modeled nor measured rates match estimated base-level rise ($4.2 \pm 0.6 \text{ mm yr}^{-1}$) during the Holocene transgression. The difference between these values is consistent with the hypothesis that the Trinity system could not keep pace with base-level rise. Hence, the system “drowned” during Holocene transgression, and the remaining topography of the underfilled valley, now comprises Galveston Bay [Simms *et al.*, 2006; Anderson *et al.*, 2008].

Although the model presented here focuses on deposition of bed material within the fluvial channel, we note that washload is also an important component of the deltaic and distal bay mud facies; consistent with many lowland fluvial-deltaic systems, washload from the Trinity River is primarily transported through the system and deposited within the downstream deltaic and distal bay depositional environments. While the initial point of delta sedimentation modeled here reflects the delta apex [Parker *et al.*, 2008a, 2008b], it is clear that based on the observed stratigraphy of the incised Trinity valley, the downstream deltaic and bay mud facies also backstep systematically with the rising base-level conditions (Figure 3). Therefore, modeling the morphodynamics of the backwater transition, and considering the migration rate of this transition due to the influence of rising base level, also reflects the tendency for the downstream, mud-dominated facies to move landward during transgression.

5.2. Trinity River Channel Avulsions and Floodplain Sedimentation During Transgression

A significant finding here is that by including a parameter that characterizes partitioning of sediment to the floodplain, there are important implications for the timing and location of modeled channel avulsions. A basic Exner model for channel sedimentation (equation (3)), which has been implemented in many other studies modeling bed evolution under the influence of nonuniform hydrodynamic conditions, limits alluvial deposition to the channel. For such a condition, avulsions are relatively frequent and essentially fixed in location regardless of the rate of base-level rise, because *all* sediment deposition is confined to the channel. Applying the channel-floodplain sediment partitioning model (equation (4)), however, renders $\sim 5\%$ of the total alluvial deposition to the channel, and the remaining $\sim 95\%$ of the bed material is assumed to be incorporated into the floodplain strata. Process wise, floodplain sedimentation occurs by two primary mechanisms: overbank sedimentation (due to both crevasse splaying and overtopping of levees with sediment-laden water) and sediment capture due to aggradation of bed material sediment that builds channel bars, combined with channel migration that captures and integrates this sediment as part of the floodplain deposit. Over the time scales expected for the infilling of an incised valley system (centuries to millennia),

sediment exchange between the channel and the floodplain via lateral migration is robust [Parker *et al.*, 2008b]. The sediment deposits for the Trinity River incised valley system, as modeled here, reflect in-channel sedimentation arising via backwater-induced deposition, which preferentially is the coarser bed material load (hence, sand [Nittrouer, 2013]). The increase in accommodation space via base-level rise will influence the streamwise location of sedimentation and also produce net sediment storage because as the channel system aggrades, sediment deposits are buried below the morphodynamic reworking depth, typically characterized as the channel depth [Straub *et al.*, 2009; Straub and Esposito, 2013; Li *et al.*, 2016].

Indeed, for the Trinity fluvial-deltaic and floodplain facies, there is an abundance of sandy deposits relative to mud, as measured by cores collected from the system (Figures 2 and 3) [McEwen, 1969; Rodriguez *et al.*, 2005]). This is particularly interesting when considering that the sediment load of the Trinity River, like many lowland fluvial systems, is primarily mud (~75%), and yet the sediment that fills the incised valley is overwhelmingly sand [McEwen, 1969; Rice, 1969]. We speculate that lateral migration coupled with rising base level is a likely mechanism to produce vertical aggradation of this sand: the production of accommodation space during transgression, combined with backwater-induced sediment deposition of bed material sediment, results in the preferential capture of sand to fill the incised valley. Due to the long advection length of mud, wash-load is not likely deposited within the incised valley fill, but instead transported to distal delta depositional regions. Hence, much of the resultant stratigraphy of the incised valley is dominated by channel sand (Figures 2 and 3).

In regard to the timing of avulsions for the Trinity system, based on the modeled conditions of base-level rise (4.3 mm yr^{-1}), a channel avulsion is produced after 3,548 model years for the minimum threshold of $0.3H$ (e.g., in accordance with Ganti *et al.* [2014]), because for higher thresholds, in-channel sedimentation cannot keep up with, let alone outpace, accommodation, in order to set up an avulsion (Figure 11). In essence, if the rate of base-level rise and production of accommodation are too great, then the channel system is immune to avulsions. Consider that by increasing the avulsion threshold to $0.4\text{--}0.6H$ (e.g., in accordance with Ganti *et al.* [2014]), avulsion conditions are only established if the base-level rise rate is no larger than 3.5 mm yr^{-1} (Figure 11). Alternatively, enhancing water discharge to $2,500 \text{ m}^3 \text{ s}^{-1}$ produces conditions of avulsion set up for the $0.3H$ threshold for base-level rise rates of 4.5 mm yr^{-1} because more sediment is supplied to the system (assuming capacity transport; Figure 10a). However, the rate of sea-level rise, as measured during the Holocene period of modeling, is constrained and is estimated not to have exceeded $4.2 \pm 0.6 \text{ mm yr}^{-1}$ (Figure 4) [Milliken *et al.*, 2008]. Given these results, we surmise that for distributary-forming channel avulsions to have occurred within the Trinity River during the period of Holocene transgression modeled here, an avulsion threshold value of $0.3H$ or smaller is required.

An important factor affecting the texture of valley fill deposits and resulting stratigraphy is the time to avulsion relative to the time that it takes a river to traverse its valley during lateral migration. As calculated by Wellmeyer *et al.* [2005], the range of lateral migration for the Trinity River was 3.0 m yr^{-1} to 6.5 m yr^{-1} between 1938 and 1964, with a time weighted average equal to 3.8 m yr^{-1} . Using this approximate value, it would require ~1,895 years for the Trinity River to traverse the width of the incised valley ($B_f = 7.2 \text{ km}$), or approximately half of the time required to meet the minimum threshold of an avulsion. During this time, approximately 1.2–2.1 m of sediment is expected to deposit, based on the values of sandy channel sedimentation produced from both measured (1.1 mm yr^{-1}) and modeled values (0.68 mm yr^{-1}). This deposit thickness represents approximately 20–40% of the bankfull channel depth ($H = 5 \text{ m}$); therefore, it is expected that subsequent migration of the channel could rework one-half to three-quarters of the previously deposited floodplain sediment, which in turn further coarsens the deposit facies toward a primarily sand facies [Rodriguez *et al.*, 2005; Parker *et al.*, 2011]. This reworking process represents yet another means to coarsen valley fill deposits and render the resulting stratigraphy as primarily composed of sand.

6. Conclusions

The stratigraphy of the Trinity valley, well constrained by previous core and seismic studies, provides unprecedented control to test a morphodynamic model that predicts patterns and mechanisms of incised valley sediment filling during Holocene transgression. An important goal of this study is to describe how backwater-induced sedimentation and the spatiotemporal set up of channel avulsions are influenced by

(1) rate of base-level rise and (2) the partitioning of sediment between the channel and the floodplain. We find that backwater-induced sediment deposition causes progradation or backstepping that is dependent on the rate of base-level rise and likely influenced by the geometry of the filling incised valley. For example, progradation of the Trinity system is predicted for rates of base-level rise less than 2 mm yr^{-1} because sediment deposition is sufficient to keep pace with the increasing accommodation space afforded by base-level rise; however, the stratigraphic evidence from the Trinity system indicates that backstepping occurred for lower rates (1.4 mm yr^{-1}) pervasive in the late Holocene because the elevation of a terrace was over topped, resulting in increased area of water inundation and sediment accommodation. Nevertheless, during the time period considered in this study (early to middle Holocene), valley geometry is constant, and it is predicted that backstepping occurred for base-level rise rates of 4.3 mm yr^{-1} due to increasing accommodation space that outpaced sediment deposition. Additionally, the rate of backstepping during this period—determined by the movement of the location of maximum backwater-induced sedimentation—is modeled to be 27 m yr^{-1} , which agrees with the stratigraphic record, which indicates a rate of $\sim 25 \text{ m yr}^{-1}$. We propose that to first order, the rate of backstepping may be constrained by the quotient of the characteristic channel bed slope and rate of base-level rise; this value, calculated for the Trinity system, is 27 m yr^{-1} .

Regarding the propensity for deltaic avulsions, we find that increasing rates of base-level rise reduce the frequency of avulsions because there is enhanced accommodation space for sedimentation, making it less likely for the channel to reach the threshold necessary to set up an avulsion (i.e., $0.3\text{--}0.6H$). Conversely, reducing the rate of base-level rise increases the frequency of channel avulsions. For the Trinity system and the conditions modeled here, it was determined that for the base-level rise rate of 4.3 mm yr^{-1} , an avulsion occurred after 3,548 model years. Furthermore, for a rate of base-level rise greater than 4.5 mm yr^{-1} , avulsions were stymied because in-channel deposition could not reach the minimum threshold required to set up an avulsion ($0.3H$).

This study uses a morphodynamic model to establish patterns of sediment deposition in order to inform the development of stratigraphy over century to millennial time scales. We demonstrate that for these time scales, it is necessary to use a modified Exner equation to account for sediment partitioning between the channel and floodplain in order to resolve differences in time and location of avulsion. In contrast, using the Exner formulation that does not include a term accounting for sediment partitioning to the floodplain—a precedent established in previous studies of backwater sedimentation over shorter temporal scales than described here—underpredicts the time required to set up an avulsion and produces a narrow range of values for the timing and location of avulsions.

Several processes contribute to deposition of relatively coarse material within lowland rivers such as the Trinity over time scales of centuries to millennia. In particular, lateral migration of the channel causes coarse bed material associated with point bars to be incorporated into valley fill deposits. Similarly, backwater-induced sedimentation selectively forces deposition of the coarser portion of the sediment load. Base-level rise produces accommodation space that results in the preservation of such deposits, building stratigraphy of the fluvial-deltaic system. As such, we predict that the early to middle Holocene deposits infilling the incised Trinity valley should be composed primarily of coarser material (in this case, sand) due to the combined effects of lateral channel migration and base-level rise. Our supposition is corroborated by the stratigraphic record: the sediment fill of the incised Trinity valley, over the time period of consideration, is almost exclusively sand. This is interesting because like most other lowland river systems, much of the total sediment load of the Trinity River is mud [McEwen, 1969; Rice, 1969]; however, that material, with its substantially long advection length, is likely transmitted downstream and deposited in the distal deltaic and marine depositional settings.

Our modeling demonstrates that partitioning of sediment between the channel and floodplain influences the timing and location of avulsions, when boundary conditions such as avulsion threshold and base-level rise rate are varied. Furthermore, our analyses suggest that understanding of fluvial-deltaic processes and deposits requires considering the combined effects of base-level rise and channel migration. The objective of this study is to build a framework whereupon other fluvial-deltaic systems that lack robust constraints on stratigraphy can be modeled using measured or inferred boundary conditions of water discharge, sediment discharge, channel width, floodplain width, grain size, channel bed slope, and sinuosity, of either modern or paleo-fluvial systems.

Notation

Variables are defined in alphabetical order. Units for each variable are defined where L is length, M is mass, and T is time. Constant input parameters are defined in Table 1 and denoted with an asterisk here.

A	cross-sectional channel area, L^2
$*B$	bankfull channel width, L
$*B_f$	floodplain width, L
$*C_f$	friction coefficient, unitless
$*D$	median grain diameter, L
Fr	Froude number, unitless
$*g$	acceleration due to gravity, $L T^{-2}$
H	bankfull flow depth, L
h	bankfull water surface elevation plus bed elevation (η), L
$*j$	intermittency, unitless
L_B	characteristic backwater length scale, L
q_t	bed material load per unit channel width, $L^2 T^{-1}$
Q_s	sediment discharge, $L^3 T^{-1}$
Q_w	water discharge, $L^3 T^{-1}$
$*R$	submerged specific gravity of sediment, unitless
$*S$	channel bed slope, unitless
t	time, T
T_A	avulsion time scale, time between avulsions, T
U	flow velocity, $L T^{-1}$
V_A	vertical aggradation rate, $L T^{-1}$
x	space, L
ζ	rate of base-level rise, $L T^{-1}$
η	bed elevation from a fixed datum, L
$*\lambda_p$	bed porosity, unitless
ζ_d	water surface elevation at the downstream end of modeled domain, L
ζ_{do}	initial water surface elevation at the downstream end of modeled domain, L
$*\rho$	water density, ML^{-3}
τ_b	boundary shear stress, $ML^{-1} T^{-2}$
$*\Omega$	sinuosity, unitless

Acknowledgments

The authors thank the Shell Center for Sustainability at Rice University for funding to the project "Stress Nexus of Coastlines Population Development, Infrastructure Security, and Morphological Dynamics of the Upper Texas Gulf Coast." Kaitlin Moran acknowledges Chevron for scholarship funding and Andrew Moodie for modeling assistance and discussions. Mauricio Perillo acknowledges ExxonMobil Upstream Research Company for support and permission to release this information. All authors acknowledge Rob Wellner for reviewing an early version of this manuscript. Furthermore, we are grateful to the reviewers of this manuscript and the Editors of JGR ES who provided valuable insight and feedback which greatly improved the quality of our manuscript. Rice University's seismic and drill acquisition was funded by the National Science Foundation, grant EAR-0107650 to J.B.A. Data may be obtained from lead author upon request.

References

- Anderson, J. B., M. A. Thomas, F. P. Siringan, and W. C. Smyth (1992), Quaternary evolution of the East Texas coast and continental shelf, in *Quaternary Coasts of the United States Marine and Lacustrine Systems*, *SEPM Spec. Publ.* 48, pp. 253–263, Soc. for Sediment. Geol., Tulsa, Okla.
- Anderson, J. B., A. Rodriguez, K. C. Abdulah, R. H. Fillon, L. A. Banfield, H. A. McKeown, and J. S. Wellner (2004), Late Quaternary stratigraphic evolution of the Northern Gulf of Mexico margin: A synthesis, *SEPM Spec. Publ.* 79, pp. 1–23, Soc. for Sediment. Geol.
- Anderson, J. B., A. B. Rodriguez, K. Milliken, and M. Taviani (2008), The Holocene evolution of the Galveston estuary complex, Texas: Evidence for rapid change in estuarine environments, in *Response of Upper Gulf Coast Estuaries to Holocene Climate Change and Sea-Level Rise*, *Geol. Soc. of Am. Spec. Pap.* 443, edited by J. B. Anderson and A. B. Rodriguez, pp. 89–104, Geol. Soc. of Am., Boulder, Colo., doi:10.1130/2008.2443(06).
- Aslan, A., and M. D. Blum (1999), Contrasting styles of Holocene avulsion, Texas Gulf Coastal Plain, USA, in *Fluvial Sedimentology VI*, edited by N. D. Smith and J. Rogers, pp. 193–209, The Int. Assoc. of Sedimentol., Oxford, U. K., doi:10.1002/9781444304213.ch15.
- Bard, E., B. Hamelin, M. Arnold, L. Montaggioni, G. Cabioch, G. Faure, and F. Rougerie (1996), Sea level record from Tahiti corals and the timing of deglacial meltwater discharge, *Nature*, 382, 241–244, doi:10.1038/382241a0.
- Blum, M. D., R. A. Morton, and J. M. Durbin (1995), "Deweyville" terraces and deposits of the Texas Gulf Coastal Plain, *Gulf Coast Assoc. Geol. Soc. Trans.*, XLV, 53–60.
- Chatanantavet, P., M. P. Lamb, and J. A. Nittrouer (2012), Backwater controls of avulsion location on deltas, *Geophys. Res. Lett.*, 39, L01402, doi:10.1029/2011GL050197.
- De Vries, M. (1965), *Considerations About Non-steady Bed-Load-Transport in Open Channels*, *Publ.* 36, Delft Hydraul. Lab., Delft, Netherlands.
- Engelund, F., and E. Hansen (1967), *A Monograph on Sediment Transport in Alluvial Streams*, Teknisk Forlag, Copenhagen.
- Failing, M. S. (1969), Comparison of Trinity River terraces and gradients with other Texas Gulf Coast rivers, in *Galveston Bay Geology*, edited by R. R. Lankford and J. J. Rogers, pp. 85–92, Houston Geol. Soc., Houston, Tex.
- Ganti, V., Z. Chu, M. P. Lamb, J. A. Nittrouer, and G. Parker (2014), Testing morphodynamic controls on the location and frequency of river avulsions on fans versus deltas: Huanghe (Yellow River), China, *Geophys. Res. Lett.*, 41, 7882–7890, doi:10.1002/2014GL061918.

- Hoyal, D. C. J. D., and B. A. Sheets (2009), Morphodynamic evolution of experimental cohesive deltas, *J. Geophys. Res.*, *114*, F02009, doi:10.1029/2007JF000882.
- Jerolmack, D. J. (2009), Conceptual framework for assessing the response of delta channel networks to Holocene sea level rise, *Quat. Sci. Rev.*, *28*, 1786–1800, doi:10.1016/j.quascirev.2009.02.015.
- Jerolmack, D. J., and D. Mohrig (2007), Conditions for branching in depositional rivers, *Geology*, *35*, 463–466, doi:10.1130/G23308A.1.
- Jerolmack, D. J., and J. B. Swenson (2007), Scaling relationships and evolution of distributary networks on wave-influenced deltas, *Geophys. Res. Lett.*, *34*, L23402, doi:10.1029/2007GL031823.
- Lamb, M. P., P. Chatanantavet, J. A. Nittrouer, D. Mohrig, and J. Shaw (2012), Backwater and river plume controls on scour upstream of river mouths: Implications for fluvio-deltaic morphodynamics, *J. Geophys. Res.*, *117*, F01002, doi:10.1029/2011JF002079.
- Lauer, J. W., and G. Parker (2008a), Modeling framework for sediment deposition, storage, and evacuation in the floodplain of a meandering river: Theory, *Water Resour. Res.*, *44*, W04425, doi:10.1029/2006WR005528.
- Lauer, J. W., and G. Parker (2008b), Modeling framework for sediment deposition, storage, and evacuation in the floodplain of a meandering river: Application to the Clark Fork River, Montana, *Water Resour. Res.*, *44*, W08404, doi:10.1029/2006WR005529.
- Lauer, J. W., and G. Parker (2008c), Net local removal of floodplain sediment by river meander migration, *Geomorphology*, *96*, 123–149, doi:10.1016/j.geomorph.2007.08.003.
- Leopold, L. B., M. G. Wolman, and J. P. Miller (1964), *Fluvial Processes in Geomorphology*, W. H. Freeman, San Francisco, Calif.
- Li, Q., L. Yu, and K. M. Straub (2016), Storage thresholds for relative sea-level signals in the stratigraphic record, *Geology*, *44*(3), 179–182, doi:10.1130/G37484.1.
- McEwen, M. C. (1969), Sedimentary facies of the Modern Trinity Delta, in *Galveston Bay Geology*, edited by R. R. Lankford and J. J. Rogers, pp. 53–77, Houston Geol. Soc., Houston, Tex.
- Milliken, K. T., J. B. Anderson, and A. B. Rodriguez (2008), A new composite Holocene sea-level curve for the northern Gulf of Mexico, in *Response of Upper Gulf Coast Estuaries to Holocene Climate Change and Sea-Level Rise*, *Geol. Soc. of Am. Spec. Pap.* *443*, edited by J. B. Anderson and A. B. Rodriguez, pp. 1–11, Geol. Soc. of Am., Boulder, Colo., doi:10.1130/2008.2443(01).
- Mohrig, D., P. L. Heller, C. Paola, and W. J. Lyons (2000), Interpreting avulsion process from ancient alluvial sequences: Guadalupe-Matarranya system (northern Spain) and Wasatch Formation (western Colorado), *GSA Bull.*, *112*(12), 1787–1803, doi:10.1130/0016-7606(2000)112<1787:IPFAA>2.0.CO;2.
- Musgrove, M., J. L. Banner, L. E. Mack, D. M. Combs, E. W. James, H. Cheng, and R. L. Edwards (2001), Geochronology of late Pleistocene to Holocene speleothems from central Texas: Implications for regional paleoclimate, *GSA Bull.*, *113*(12), 1532–1543, doi:10.1130/0016-7606(2001)113<1532:GOLPTH>2.0.CO;2.
- Nittrouer, J. A. (2013), Backwater hydrodynamics and sediment transport in the lowermost Mississippi River Delta: Implications for the development of fluvial-deltaic landforms in a large lowland river, in *Deltas: Landforms, Ecosystems, and Human Activities*, *IAHS Publ.* *358*, edited by G. Young and G. M. E. Perillo, pp. 48–61, Gothenburg, Sweden.
- Nittrouer, J. A., J. Shaw, M. P. Lamb, and D. Mohrig (2012), Spatial and temporal trends for water-flow velocity and bed-material sediment transport in the lower Mississippi River, *GSA Bull.*, *124*(3/4), 400–414, doi:10.1130/B30497.1.
- Paola, C., and V. R. Voller (2005), A generalized Exner equation for sediment mass balance, *J. Geophys. Res.*, *110*, F04014, doi:10.1029/2004JF000274.
- Parker, G. (2004), 1D sediment transport morphodynamics with applications to rivers and turbidity currents, Univ. of Ill. at Urbana-Champaign. [Available at http://hydrolab.illinois.edu/people/parkerg/morphodynamics_e-book.htm.]
- Parker, G., C. Paola, K. X. Whipple, and D. Mohrig (1998a), Alluvial fans formed by channelized fluvial and sheet flow. I: Theory, *J. Hydraul. Eng.*, *124*(10), 985–995.
- Parker, G., C. Paola, K. X. Whipple, D. Mohrig, C. M. Toro-Escobar, M. Halverson, and T. W. Skoglund (1998b), Alluvial fans formed by channelized fluvial and sheet flow. II: Application, *J. Hydraul. Eng.*, *124*(10), 996–1004.
- Parker, G., T. Muto, Y. Akamatsu, W. E. Dietrich, and J. W. Lauer (2008a), Unravelling the conundrum of river response to rising sea-level from laboratory to field. Part I: Laboratory experiments, *Sedimentology*, *55*, 1643–1655, doi:10.1111/j.1365-3091.2008.00961.x.
- Parker, G., T. Muto, Y. Akamatsu, W. E. Dietrich, and J. W. Lauer (2008b), Unravelling the conundrum of river response to rising sea-level from laboratory to field. Part II. The Fly-Strickland River system, Papua New Guinea, *Sedimentology*, *55*, 1657–1686, doi:10.1111/j.1365-3091.2008.00962.x.
- Parker, G., Y. Shimizu, G. V. Wilkerson, E. C. Eke, J. D. Abad, J. W. Lauer, C. Paola, W. E. Dietrich, and V. R. Voller (2011), A new framework for modeling the migration of meandering rivers, *Earth Surf. Processes Landforms*, *36*, 70–86, doi:10.1002/esp.2113.
- Phillips, J. D., M. C. Slattery, and Z. A. Musselman (2004), Dam-to-delta sediment inputs and storage in the lower Trinity River, Texas, *Geomorphology*, *62*, 17–34, doi:10.1016/j.geomorph.2004.02.004.
- Reh Kemper, L. J., M. C. McEwen, R. R. Lankford, and J. J. Rogers (1969), Data sheets, Trinity River Delta, in *Galveston Bay Geology*, edited by R. R. Lankford and J. J. Rogers, pp. 136–141, Houston Geol. Soc., Houston, Tex.
- Rice, R. H. (1969), Suspended load of the Trinity River, in *Galveston Bay Geology*, edited by R. R. Lankford and J. J. Rogers, pp. 78–84, Houston Geol. Soc., Houston, Tex.
- Rodriguez, A. B., J. B. Anderson, and A. R. Simms (2005), Terrace inundation as an autocyclic mechanism for parasequence formation: Galveston Estuary, Texas, U.S.A., *J. Sediment. Res.*, *75*, 608–620, doi:10.2110/jsr.2005.050.
- Simms, A. R., J. B. Anderson, Z. P. Taha, and A. B. Rodriguez (2006), Overfilled versus underfilled incised valleys: Examples from the Quaternary Gulf of Mexico, in *Incised Valleys in Time and Space*, *SEPM Spec. Publ.* *85*, edited by R. W. Dalrymple, D. A. Leckie, and R. W. Tillman, pp. 117–139, SEPM, Tulsa, Okla., doi:10.2110/pec.06.85.
- Simms, A. R., J. B. Anderson, K. T. Milliken, Z. P. Taha, and J. S. Wellner (2007), Geomorphology and age of the oxygen isotope stage 2 (last lowstand) sequence boundary on the northwestern Gulf of Mexico continental shelf, in *Seismic Geomorphology: Applications to Hydrocarbon Exploration and Production*, *Spec. Publ.* *277*, edited by R. J. Davies et al., pp. 29–46, Geol. Soc., London.
- Simms, A. R., J. B. Anderson, R. DeWitt, K. Lambeck, and A. Purcell (2013), Quantifying rates of coastal subsidence since the last interglacial and the role of sediment loading, *Global Planet. Change*, *111*, 296–308, doi:10.1016/j.gloplacha.2013.10.002.
- Slingerland, R., and N. D. Smith (2004), River avulsions and their deposits, *Annu. Rev. Earth Planet. Sci.*, *32*, 257–285, doi:10.1146/annurev.earth.32.101802.120201.
- Smith, V. B. (2012), Geomorphology of a coastal sand-bed river: Lower Trinity River, Texas, PhD dissertation, Jackson Sch. of Geosci., The Univ. of Texas, Austin.
- Straub, K. M., and C. R. Esposito (2013), Influence of water and sediment supply on the stratigraphic record of alluvial fans and deltas: Process controls on stratigraphic completeness, *J. Geophys. Res. Earth Surf.*, *118*, 625–637, doi:10.1002/jgrf.20061.
- Straub, K. M., C. Paola, D. Mohrig, M. A. Wolinsky, and T. George (2009), Compensational stacking of channelized sedimentary deposits, *J. Sediment. Res.*, *79*, 673–688, doi:10.2110/jsr.2009.070.

- Thomas, M. A., and J. B. Anderson (1988), The effect and mechanism of episodic sea level events: The record preserved within late Wisconsinian-Holocene incised valley-fill sequences, *Gulf Coast Assoc. Geol. Soc. Trans.*, *XXXVIII*, 399–406.
- Thomas, M. A., and J. B. Anderson (1994), Sea-level controls on the facies architecture of the Trinity/Sabine incised-valley system, Texas continental shelf, in *Incised-Valley Systems: Origin and Sedimentary Sequences*, *SEPM Spec. Publ. 51*, edited by R. W. Dalrymple, R. Boyd, and B. A. Zaitlin, pp. 63–82, SEPM, Tulsa, Okla., doi:10.2110/sepm51.104.
- Viparelli, E., J. A. Nittrouer, and G. Parker (2015), Modeling flow and sediment transport dynamics in the lowermost Mississippi River, Louisiana, USA, with an upstream alluvial-bedrock transition and a downstream bedrock-alluvial transition: Implications for land building using engineered diversions, *J. Geophys. Res. Earth Surf.*, *120*, 534–563, doi:10.1002/2014JF003257.
- Weight, R. W., J. B. Anderson, and R. Fernandez (2011), Rapid mud accumulation on the central Texas shelf linked to climate change and sea-level rise, *J. Sediment. Res.*, *81*, 743–764, doi:10.2110/jsr.2011.57.
- Wellmeyer, J. L., M. C. Slattery, and J. D. Phillips (2005), Quantifying downstream impacts of impoundment on flow regime and channel planform, lower Trinity River, Texas, *Geomorphology*, *69*, 1–13, doi:10.1016/j.geomorph.2004.09.034.
- Wolman, M. G., and J. P. Miller (1960), Magnitude and frequency of forces in geomorphic processes, *J. Geol.*, *68*, 54–74.